THE JOURNAL OF PHYSICAL CHEMISTRY A

Article

pubs.acs.org/JPCA

Complexes between Planar Boron Clusters and Transition Metals: A Photoelectron Spectroscopy and Ab Initio Study of CoB_{12}^- and RhB_{12}^-

Ivan A. Popov,[†] Wei-Li Li,[‡] Zachary A. Piazza,[‡] Alexander I. Boldyrev,*[,†] and Lai-Sheng Wang*[,‡]

[†]Department of Chemistry and Biochemistry, Utah State University, Logan, Utah, 84322, United States

[‡]Department of Chemistry, Brown University, Providence, Rhode Island, 02912, United States

Supporting Information

ABSTRACT: Small boron clusters are known to be planar, and may be used as ligands to form novel coordination complexes with transition metals. Here we report a combined photoelectron spectroscopy and ab initio study of CoB_{12}^- and RhB_{12}^-. Photoelectron spectra of the two doped-B_{12} clusters show similar spectral patterns, suggesting they have similar structures. Global minimum searches reveal that both CoB_{12}^- and RhB_{12}^- possess half-sandwich-type structures with the quasi-planar B_{12} moiety coordinating to the metal atom. The B_{12} ligand is found to have similar structure as the bare B_{12} cluster with C_{3v} symmetry. Structures with Co or Rh inserted into the quasi-planar boron framework are found to be much higher in energy. Chemical bonding analyses of the two B_{12} half sandwiches reveal two sets of σ bonds on the boron unit: nine classical two-center−two-electron (2c−2e) σ bonds on the periphery of the B_{12} unit and four 3c−2e σ bonds within the boron unit. Both σ and π bonds are found between the metal and the B_{12} ligand: three M−B single σ bonds and one delocalized 4c−2e π bond. The exposed metal sites in these complexes can be further coordinated by other ligands or become reaction centers as model catalysts.

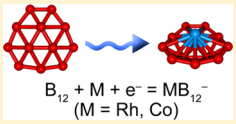

I. INTRODUCTION

Boron has one electron less than its valence orbitals; this electron deficiency results in very different chemistries for boron relative to carbon. While small carbon clusters are chains or rings,[1] small boron clusters (B_n) have been found to be planar or quasi-planar (2D) up to at least 24 atoms as anions[2−10] or up to 16 atoms as cations.[11] Direct experimental studies of neutral boron clusters have been challenging, and the 2D−3D transition has not been experimentally confirmed. Even though neutral B_{20} was found computationally to have a 3D double ring global minimum,[10,12] recent infrared experiment failed to detect this structure.[13] Similarly, the proposed 3D structure for B_{14} (ref 14) runs counter to the recent infrared experiment that neutral B_{11}, B_{16}, and B_{17} are planar.[13] In addition to their interesting chemical bonding, small planar boron clusters may be used as novel ligands or building blocks for new nanostructures. Among the small boron clusters, the closed-shell B_3^-, B_8^{2-}, B_9^-, B_{10}, B_{11}^-, and B_{12} have been suggested to be the best candidates as new inorganic ligands or building blocks,[15,16] because they are all aromatic according to the Hückel's rule with $4N + 2$ π electrons.

Theoretical studies suggested that the doubly aromatic B_3^- may form stable $M^+[B_3^-]$ (M = Li−Cs) ionic complexes.[17] Anionic complexes of $Li^+[B_6^{2-}]$ and $Li^+[B_8^{2-}]$ have been observed experimentally and studied by photoelectron spectroscopy (PES) and theoretical calculations.[16,18] The boron cluster motifs in these ionic complexes have almost the same structures and electronic properties as the corresponding bare clusters. Aluminum-doped B_7 and B_8 clusters, AlB_7^- and AlB_8^-, were found to have umbrella-type $Al^{2+}[B_7^{3-}]$ and $Al^+[B_8^{2-}]$ structures in a combined PES and theoretical study.[19] The stability of these clusters was attributed to the double aromaticity of B_7^{3-} and B_8^{2-}. More interestingly, transition-metal-doped B_8, B_9, and B_{10} clusters have been discovered to form a series of novel borometallic molecular wheels:[20] Co©B_8^- and Ru©B_9^-,[21] M©B_9 and M©B_9^- (M = Rh, Ir),[22] Ta©B_{10}^- and Nb©B_{10}^-,[23] and Fe©B_8^- and Fe©B_9^-.[24] The © symbol was proposed to designate the central position of the doped atom in the planar monocyclic structures of the new borometallic complexes.[21] Geometric and electronic factors in the rational design of the novel borometallic molecular wheels have been investigated.[20,25] Very recently,[26] the structures and chemical bonding of a series of TaB_n^- (n = 3−8) clusters were studied to probe the formation mechanisms of the Ta©B_{10}^- molecular wheel, which holds the highest coordination number for a metal complex in planar geometry.[23,27] Theoretical investigations on X©B_nH_n (X = B^+, Be; n = 5−8) and M©B_nH_n (M = V^-, Cr, Mn^+) have also been reported recently.[28,29]

Interestingly, triple-decker complexes containing planar B_nH_n units, such as $(Cp^*Re)_2B_nX_n$ (n = 5−7; X = Cl or H), were synthesized previously and characterized structurally;[30,31] the two metal atoms were thought to contribute six electrons to the B_6X_6 or B_5X_5 (X = H or Cl) motifs. Bare planar B_6 rings embedded in one-dimensional Ti_7 wheels were found in the crystal structure of a solid-state phase of $Ti_7Rh_4Ir_2B_8$.[32] Very recently, the planar B_6 ring has been found to be sandwiched between two Ta atoms in the Ta_2B_6 cluster.[33] Thus, planar

Special Issue: A. W. Castleman, Jr. Festschrift

Received: December 3, 2013
Revised: January 14, 2014
Published: January 15, 2014

dx.doi.org/10.1021/jp411867q | J. Phys. Chem. A 2014, 118, 8098−8105

boron-based fragments can indeed be viable ligands in different sandwich complexes and may play an important role in the further development of boron chemistry.

In our studies of the $M©B_n^-$ molecular wheels, the position of the metal atom has been found to depend on two factors: the electronic requirement to fulfill double aromaticity and the geometrical factor depending on the size of the metal atom.[20,34] The geometrical factor requires that the central atom fits into the cavity of a monocyclic ring. The electronic factor requires the right number of valence electrons to achieve electronic stability of the high-symmetry structure. It was shown that a systematic destabilization of the $M©B_{10}^-$ molecular wheel going up the periodic table from Ta to V is due to the decreasing metal atom size.[34] The smaller atomic size and the more contracted 3d orbitals make the V atom energetically unfavorable to fit inside a B_{10} ring to form a stable $V©B_{10}^-$ molecular wheel. Hence, VB_{10}^- has a boat-like structure with the V bonded above a B_{10} unit, which resembles the structure of the bare B_{10} cluster. This is the largest boron cluster, observed thus far to act as a ligand.

On the basis of these ideas, one would expect to find similar clusters with a transition metal atom coordinated in the same manner with respect to a quasiplanar boron framework. The boron cluster should maintain a similar planar geometry to that of the undoped boron cluster of the same stoichiometry. Then, the question is: what is the largest planar boron ligand that will maintain its structure in a half-sandwich-type complex with a metal atom? A good candidate is the highly stable quasiplanar B_{12}, an aromatic cluster with a large HOMO−LUMO gap, as revealed from the photoelectron spectra of B_{12}^-.[3] It has a very interesting bowl structure: a nine-membered outer ring and an inner B_3 triangle that is slightly out of plane. Theoretical calculations suggested that monometal doped B_{12} clusters could form the half-sandwich clusters.[35,36] The B_{12} fragment in such doped clusters has the C_{3v} symmetry as the bare B_{12} cluster, but is more curved. However, there has been no experimental evidence of such structures.

In the current study, we report two transition-metal-doped B_{12} clusters, i.e., RhB_{12}^- and CoB_{12}^-, which are characterized by photoelectron spectroscopy and *ab initio* calculations. The photoelectron spectra of both clusters show relatively simple spectral patterns, suggesting they may have similar high symmetry structures. Extensive structural searches found that the half sandwich structures are indeed the global minima for both clusters. Chemical bonding analyses showed that the B_{12} motif maintains similar structures as the bare cluster, but becomes slightly more curved toward to the metal atoms. Both σ and π bonds are found between the B_{12} motif and the metal atom.

II. EXPERIMENTAL AND THEORETICAL METHODS

A. Experimental Method. The experiment was carried out using a magnetic-bottle PES apparatus equipped with a laser vaporization cluster source, the details of which have been described elsewhere.[37] Briefly, the MB_{12}^- clusters were generated by laser ablation of a cold-pressed target composed of Co (or Rh) and isotopically enriched ^{10}B, balanced by Bi, which acted as a binder and also provided a convenient calibrant (Bi^-) for the photoelectron spectra. Clusters formed in the nozzle were entrained in a He carrier gas and underwent a supersonic expansion to form a collimated cluster beam. The He carrier gas was seeded with 5% Ar, which was found to provide better cooling for the entrained clusters.[38,39] The anionic clusters were extracted from the collimated cluster beam and analyzed by a time-of-fight mass spectrometer. The MB_{12}^- clusters of current interest were mass-selected and decelerated before photodetached by a laser beam operated at 193 nm (6.424 eV) from an ArF excimer laser and 266 nm (4.661 eV) from a Nd:YAG laser. Photoelectrons were collected at nearly 100% efficiency by the magnetic bottle and analyzed in a 3.5 m long flight tube. The resolution of the apparatus, $\Delta E_k/E_k$, was better than 2.5%, i.e., ~25 meV for 1 eV electrons.

B. Theoretical Methods. Unbiased searches for the global minima of CoB_{12}^- and RhB_{12}^- with different spin states (singlet and triplet) were performed using the Coalescence Kick (CK) program, the details of which can be found in ref 16. Approximately 5000 trial structures were generated for each cluster in a particular spin state followed by geometry optimization at PBE0/LANL2DZ level of theory.[40−42] The low energy isomers (ΔE < 45 kcal/mol) were then reoptimized at PBE0/M/Stuttgart/B/aug-cc-pVTZ[43−47] (M = Co, Rh). Single-point calculations for selected isomers were further performed using the CCSD(T)/M/Stuttgart/B/aug-cc-pVTZ//PBE0/M/Stuttgart/B/aug-cc-pVTZ method. For each structure, vibrational frequencies were calculated and imaginary frequencies were followed to ensure that it corresponded to a true minimum on the potential energy surface. The restricted open-shell calculations were performed for the open-shell isomers at the ROCCSD(T)/M/Stuttgart/B/aug-cc-pVTZ//PBE0/M/Stuttgart/B/aug-cc-pVTZ level of theory.

Vertical detachment energies (VDEs) of the global minimum structures were calculated at the TD-DFT/M/Stuttgart/B/aug-cc-pVTZ (DFT = PBE0 for RhB_{12}; BP86[48,49] for CoB_{12}) level of theory to compare with the experimental data. The BP86 functional was found previously to give superior results for energetic properties for clusters involving 3d transition metals.[34,50,51] To be precise, all the VDEs of CoB_{12}^- were calculated using the TD-BP86 method, which is based on the nonhybrid BP86 functional. On the other hand, the PBE0 functional, which involved a 1:3 mixture of DFT and exact exchange energies, was utilized to obtain the VDEs of RhB_{12}^-. For each cluster, the first VDE was calculated as the difference in energy between the lowest anionic state and the lowest neutral state at the geometry of the anion. Then, vertical excitation energies of the neutral species calculated at the TD-DFT levels were added to the first VDE to approximate the second and higher VDEs. Even though we were not able to compute VDEs for both clusters at the same level of theory, we found good agreement between the experimental and theoretical VDEs in each case (*vide infra*).

Chemical bonding analyses were done on the global minima of CoB_{12}^- and RhB_{12}^- using the adaptive natural density partitioning (AdNDP) method,[52] which has been successfully used to provide insight into the chemical bonding of not only boron clusters, but also of boron and carbon 2D materials.[53−55] The AdNDP method analyzes the first-order reduced density matrix in order to obtain its local block eigenfunctions with optimal convergence properties for an electron density description. The obtained local blocks correspond to sets of n-atoms (n ranging from one to the total number of atoms in the molecule) that are tested for the presence of n-electron objects [n-center two-electron (nc−2e) bonds]. The AdNDP method initially searches for core electron pairs and lone pairs (1c−2e), then 2c−2e, 3c−2e, ..., and finally up to nc−2e bonds.

dx.doi.org/10.1021/jp411867q | J. Phys. Chem. A 2014, 118, 8098−8105

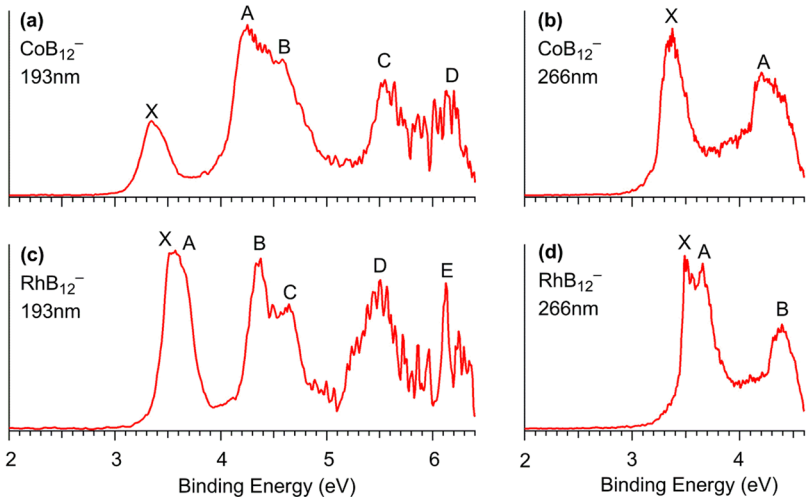

Figure 1. Photoelectron spectra of CoB_{12}^- (a,b) and RhB_{12}^- (c,d) at 193 nm (6.424 eV) and 266 nm (4.661 eV). The 266 nm spectra offer better spectral resolution than the 193 nm spectra.

Table 1. Observed VDEs of CoB_{12}^- and RhB_{12}^- Compared with the Calculated Values*

Feature	VDE (exp)[a]	Final State and Electronic Configuration	VDE
		CoB_{12}^- (C_{3v}, $^1A_1$)[b]	TD(BP86)
X	3.37 (4)	^2E … $1a_2^2 3a_1^2 4a_1^2 3e^4 4e^4 5a_1^2 5e^4 6a_1^2 6e^4 7e^4 8e^3$	3.39
A	4.20 (4)	^2E … $1a_2^2 3a_1^2 4a_1^2 3e^4 4e^4 5a_1^2 5e^4 6a_1^2 6e^4 7e^3 8e^4$	4.28
B	4.58 (5)	^2E … $1a_2^2 3a_1^2 4a_1^2 3e^4 4e^4 5a_1^2 5e^4 6a_1^2 6e^3 7e^4 8e^4$	4.52
		$^2A_1$ … $1a_2^2 3a_1^2 4a_1^2 3e^4 4e^4 5a_1^2 5e^4 6a_1^1 6e^4 7e^4 8e^4$	4.88
C	5.55 (4)	^2E … $1a_2^2 3a_1^2 4a_1^2 3e^4 4e^4 5a_1^2 5e^3 6a_1^2 6e^4 7e^4 8e^4$	5.72
		$^2A_1$ … $1a_2^2 3a_1^2 4a_1^2 3e^4 4e^4 5a_1^1 5e^4 6a_1^2 6e^4 7e^4 8e^4$	5.88
D	~6.1	^2E … $1a_2^2 3a_1^2 4a_1^2 3e^4 4e^3 5a_1^2 5e^4 6e^4 6a_1^2 7e^4 8e^4$	6.21
		RhB_{12}^- (C_{3v}, $^1A_1$)[c]	TD(PBE0)
X	3.49 (4)	^2E … $3e^4 4e^4 5e^4 5a_1^2 6e^4 6a_1^2 7e^4 8e^3$	3.42
A	3.65 (4)[d]		
B	4.39 (4)	^2E … $3e^4 4e^4 5e^4 5a_1^2 6e^4 6a_1^2 7e^3 8e^4$	4.59
C	4.64 (5)[e]		
D	~5.5	^2E … $3e^4 4e^4 5e^4 5a_1^2 6e^3 6a_1^2 7e^4 8e^4$	5.26
		$^2A_1$ … $3e^4 4e^4 5e^4 5a_1^2 6e^4 6a_1^1 7e^4 8e^4$	5.41
E	~6.2	^2E … $3e^4 4e^4 5e^3 5a_1^2 6e^4 6a_1^2 7e^4 8e^4$	6.34

*All energies are in eV. [a]Numbers in parentheses represent the uncertainty in the last digit. [b]The VDEs were calculated at TD-BP86/Co/Stuttgart/B/aug-cc-pVTZ//BP86/Co/Stuttgart/B/aug-cc-pVTZ. [c]The VDEs were calculated at TD-PBE0/Rh/Stuttgart/B/aug-cc-pVTZ//PBE0/Rh/Stuttgart/B/aug-cc-pVTZ. [d]This feature is assigned to the second spin−orbit component of the ^2E ground state. [e]This is assigned to the Jahn−Teller or spin−orbit splitting of the ^2E excited state.

At every step, the density matrix is depleted of the density corresponding to the appropriate bonding elements. The user-directed form of the AdNDP analysis can be applied to specified molecular fragments and is analogous to the directed search option of the standard natural bond orbital (NBO) code.[56,57] AdNDP accepts only those bonding elements whose occupation numbers (ONs) exceed a specified threshold value, which is usually chosen to be close to 2.00 lel. We used the PBE0/LANL2DZ level of theory for the AdNDP calculations.

To estimate the spin−orbit splitting expected for each electronic transition for the MB_{12}^- clusters single point calculations were conducted with the PBE0/QZ4P[58] functional and basis set combination using the zero-order relativistic approximation (ZORA) as implemented in the ADF program package.[59−61] All geometry optimization, TD-DFT, RCCSD-(T), and ROCSSD(T) were performed using the GAUSSIAN 09 program.[62] Molecular structure visualization was done using the MOLDEN 3.4[63] and Chemcraft programs.[64] Molecular orbital (MO) visualization was performed using MOLEKEL 5.4.0.8.[65]

dx.doi.org/10.1021/jp411867q | J. Phys. Chem. A 2014, 118, 8098−8105

III. EXPERIMENTAL RESULTS

The photoelectron spectra of CoB_{12}^- and RhB_{12}^- at two different photon energies are shown in Figure 1. The spectra measured at 193 nm reveal more detachment features, while those obtained at 266 nm provide slightly better spectral resolution. The PES bands are labeled with letters (X, A, B, ...) and the VDEs for all observed bands are given in Table 1, where they are compared with the calculated VDEs.

A. CoB_{12}^-. The 193 nm spectrum (Figure 1a) exhibits a relatively simple spectral pattern with five resolved bands, labeled as X and A–D. All the PES bands are quite broad, suggesting significant geometry changes between the anion and the neutral states or overlapping of multiple detachment transitions. The X band represents the detachment transition from the ground state of CoB_{12}^- to that of neutral CoB_{12}. The VDE of the X band is measured as 3.37 eV from the peak maximum in the 266 nm spectrum (Figure 1b). The ADE is evaluated to be 3.23 eV by drawing a straight line along the leading edge of band X and then adding the instrumental resolution to the intersection with the binding energy axis. The VDE of band A is measured as 4.20 eV from the 266 nm spectrum, whereas the VDEs of band B, C, and D are obtained from the 193 nm spectrum as 4.58 eV, 5.55 eV, and ~6.1 eV, respectively. The band D is tentatively assigned due to the low signal-to-noise ratio in the high binding energy side of the 193 spectrum.

B. RhB_{12}^-. The spectra of RhB_{12}^- are similar to those of CoB_{12}^- except the relative intensities and splittings of certain spectral bands. For example, the lowest binding energy band of RhB_{12}^- at 193 nm (Figure 1c) is the most intense band and it is resolved into two relatively sharp features (X and A) in the 266 nm spectrum (Figure 1d). This splitting could be due to either the Jahn–Teller or spin–orbit (SO) effects. The VDE of the lowest binding energy band X is measured to be 3.49 eV and its ADE is measured to be 3.45 eV from the 266 nm spectrum. Feature A is split from band X by 0.16 eV with a VDE of 3.65 eV. The VDEs of the next two bands B and C are measured to be 4.39 and 4.64 eV, respectively. Band D at ~5.5 eV is fairly broad and likely consists of several overlapping detachment channels. Similar to the 193 nm spectrum of CoB_{12}^-, the signal-to-noise ratio of the high binding energy side of the 193 nm spectrum of RhB_{12}^- is also poor and the sharp peak at 6.13 eV cannot be assigned as a single vibronic transition. A VDE of ~6.2 eV is tentatively identified for the band E, similar to the band D in the CoB_{12}^- case.

IV. THEORETICAL RESULTS

A. Global Minimum Searches for CoB_{12}^- and RhB_{12}^-. The 10 energetically lowest lying isomers of MB_{12}^- at PBE0/M/Stuttgart/B/aug-cc-pVTZ are presented in the Supporting Information: all the isomers found within 30 kcal/mol with respect to the global minimum for CoB_{12}^- (Figure S1), and within 45 kcal/mol for RhB_{12}^- (Figure S2). All these structures represent minima on the potential energy surfaces. The $\langle S^2 \rangle$ values were found to be in the range of 2.02–2.20 for all the DFT calculations. Subsequently, more accurate single-point calculations were performed at CCSD(T)/M/Stuttgart/B/aug-cc-pVTZ//PBE0/M/Stuttgart/B/aug-cc-pVTZ (M = Co, Rh). The restricted open-shell formalism was used to give the proper $\langle S^2 \rangle$ value for the open-shell species at the CCSD(T) level of theory. In the case of RhB_{12}^-, the second isomer (C_s, $^1A'$, II in Figure S2) turned out to be 18.0 and 15.4 kcal/mol higher in energy than the global minimum isomer I (C_{3v}, $^1A_1$) at the PBE0 and CCSD(T) levels of theory, respectively. Thus, isomer II was not expected to be present experimentally. All the other isomers found by the CK searches for RhB_{12}^- represent high-energy structures (Figure S2). For CoB_{12}^-, the second isomer (C_s, $^3A''$, II in Figure S1) is 4.8 kcal/mol higher in energy than the global minimum isomer I (C_{3v}, $^1A_1$) at PBE0 level. We do not present results at the CCSD(T) level for the CoB_{12}^- clusters, because we found the values of the T_1 diagnostic (T_1 = 0.39)[66–68] and NORM(A) (1.70) were quite large for CoB_{12}^- in comparison to those for RhB_{12}^- [T_1 = 0.12 and NORM(A) = 1.34]. Hence, the coupled cluster relative energy ordering should be treated with caution for CoB_{12}^-. These results suggested that the true wave functions for the structures of CoB_{12}^- might be more accurately described by multiconfigurational reference states. Nevertheless, on the basis of the results for RhB_{12}^-, the PBE0 energies for CoB_{12}^- should be reasonably reliable and the second isomer should be negligible experimentally.

B. The Global Minima for CoB_{12}^- and RhB_{12}^-. The global minimum structures of CoB_{12}^- and RhB_{12}^- are similar, as shown in Figure 2. Both anions possess C_{3v} symmetry with a half sandwich structure, in which the B_{12} moiety is similar to the bare B_{12} cluster. The B_{12} framework is slightly puckered to achieve optimal interactions with the metal atoms. In RhB_{12}^-, the distance between Rh and the three inner boron atoms is slightly larger (2.09 Å) than for Co (1.97 Å), consistent with the atomic radii of the two metal atoms. All B–B bond distances in RhB_{12}^- and CoB_{12}^- are similar to those in the bare B_{12} cluster (Figure 3a). The only significant difference comes from the curvature of the B_{12} framework: the peripheral atoms bend out of the plane of the inner triangle by 0.70 Å and 0.88 Å in RhB_{12}^-, by 0.74 Å and 0.94 Å in CoB_{12}^-, whereas in pure B_{12} these distances are 0.22 Å and 0.35 Å, respectively.

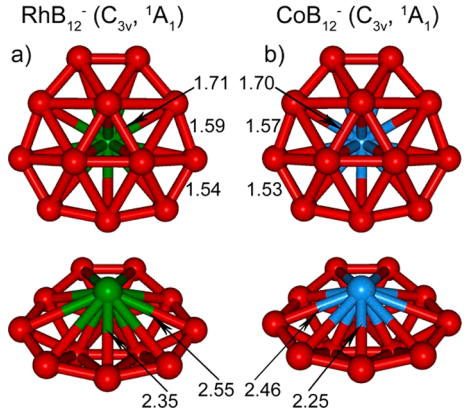

Figure 2. Two views of the global minimum structures of (a) RhB_{12}^- and (b) CoB_{12}^-. Their point group symmetries and spectroscopic states are shown in parentheses. Bond lengths are given in Å.

The inner atoms in the planar B_{13}^+ cluster with a 9-atom periphery[69,70] have been shown previously to be fluxional with an internal rotation barrier of only 0.1 kcal/mol,[71] similar to that in the planar B_{19}^- cluster.[6,72] The facile internal rotation in B_{13}^+ and B_{19}^- is akin to "molecular Wankel motors".[71,72] Figure 3 shows results of the internal rotation in the pure B_{12} cluster, compared with that in MB_{12}^-. In both cases, the 60° rotation of the inner B_3 triangle results in a transition state, corresponding to a saddle point with an imaginary frequency. It seems that

dx.doi.org/10.1021/jp411867q | J. Phys. Chem. A 2014, 118, 8098–8105

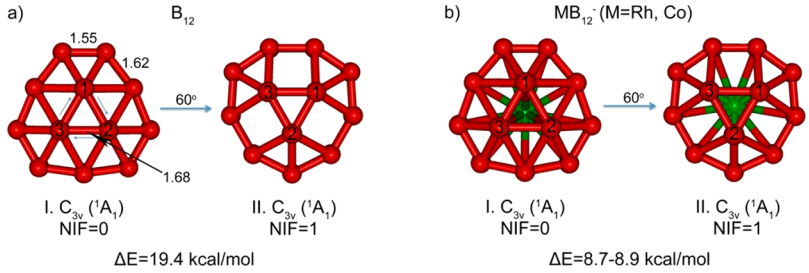

Figure 3. Rotational barriers of the inner boron triangle with respect to the outer ring for B_{12} and MB_{12}^- obtained at the PBE0/aug-cc-pVTZ and PBE0/M/Stuttgart/B/aug-cc-pVTZ (M═Rh, Co) levels of theory, respectively. NIF denotes number of imaginary frequencies.

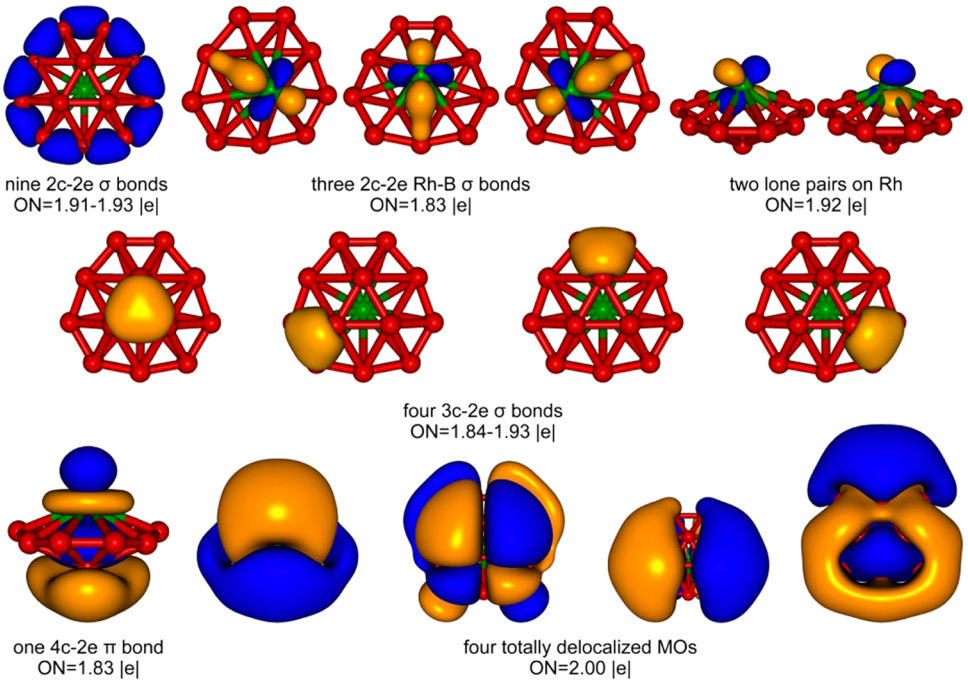

Figure 4. AdNDP analysis for RhB_{12}^-. ON denotes the occupation number and is equal to 2.00 |e| in the ideal case.

complexion of B_{12} with a metal atom significantly reduces the barrier of the internal rotation.

V. COMPARISON BETWEEN EXPERIMENT AND THEORY

A. CoB_{12}^-. The global minimum of CoB_{12}^- is closed shell with a $^1A_1$ ground state and thus only doublet final states are expected upon one electron detachment. The HOMO (8e) of CoB_{12}^- is doubly degenerate, resulting in a ^2E final state upon one electron detachment (Table 1). This doubly degenerate final state is unstable against Jahn−Teller distortion and it can also be split by spin−orbit effects, consistent with the broad width of the X band (Figure 1b). The calculated first VDE of 3.39 eV agrees well with the 3.37 eV VDE measured for the X band (Table 1). The calculated ADE of 3.22 eV is also in good agreement with the measured value of 3.23 eV. The next three detachment channels from HOMO-1 (7e), HOMO-2 (6e), and HOMO-3 ($6a_1$) give rise to calculated VDEs of 4.28, 4.52, and 4.88 eV, respectively, which are fairly close to each other and are in good agreement with the VDEs for the broad and overlapping bands (4 to 5 eV) labeled A and B (Figure 1a). Following a large energy gap, the next two detachment channels from the 5e and $5a_1$ orbitals yield VDEs very close to each other and are assigned to band C. The detachment from the 4e orbital has a calculated VDE of 6.21 eV, in good agreement with that of band D at ∼6.1 eV. Overall, the calculated VDEs and spectral pattern are in excellent agreement with the experimental PES data, lending considerable credence to the C_{3v} global minimum of CoB_{12}^-.

B. RhB_{12}^-. The electronic structure and MO configuration of RhB_{12}^- (Table 1) are similar to those of CoB_{12}^-. Electron detachment from the doubly degenerate HOMO (8e) produces the ^2E neutral ground state with a calculated VDE of 3.42 eV, which agrees well with that of band X at 3.49 eV. However, the second detachment channel from HOMO-1 (7e) yielded a calculated VDE of 4.59 eV and cannot be responsible for band A. Comparison of the spectra of RhB_{12}^- with that of CoB_{12}^- suggests that band A in RhB_{12}^- must come from the SO splitting of the ^2E neutral ground state. Spin−orbit calculations show a SO splitting of 0.1 eV, consistent with the energy difference of bands X and A (0.16 eV). The VDE of electron detachment from HOMO-2 (7e) is calculated at 4.59 eV with negligible SO splitting (<0.01 eV). This VDE agrees well with the VDEs of bands B (4.39 eV) and C (4.64 eV), which are tentatively assigned to the Jahn−Teller splitting of the excited ^2E final state (Table 1). Similar Jahn−Teller splitting from detachment of an electron from the 7e orbital was expected to occur in the CoB_{12}^- case. However, as shown above, the 6e and

dx.doi.org/10.1021/jp411867q | J. Phys. Chem. A 2014, 118, 8098−8105

$5a_1$ detachment channels have very close VDEs, overlapping with that of the 7e orbital and preventing a clear observation of the Jahn−Teller splitting in the CoB_{12}^- spectrum. In the case of RhB_{12}^-, detachments from the 6e and $5a_1$ orbitals yield much higher VDEs (5.26 and 5.41 eV, respectively), compared with those in the CoB_{12}^- case, corresponding to the broad D band at ∼5.5 eV (Figure 1c and Table 1). Finally, detachment from the 5e orbital results in a calculated VDE of 6.34 eV, consistent with band D at ∼6.2 eV. Even though the Jahn−Teller splitting cannot be treated in the current calculations, the overall agreement between the theoretical results and the experimental data is quite good, in particular, by comparing the results between RhB_{12}^- and CoB_{12}^-, confirming the C_{3v} global minimum of RhB_{12}^-.

VI. CHEMICAL BONDING ANALYSES

The chemical bonding of RhB_{12}^- was analyzed using the AdNDP method, as shown in Figure 4. The AdNDP analysis for CoB_{12}^- is almost identical and thus is not shown. As given in Figure 4, the occupation numbers of all the identified bonds range from 1.83 to 2.00 lel.

The chemical bonding of the B_{12} moiety is reminiscent of the bare quasi-planar B_{12} cluster,[3] including nine 2c−2e B−B σ bonds on the outer ring and four 3c−2e σ bonds delocalized over the surface of the B_{12} moiety. All the π bonds in the B_{12} moiety are used to form bonds with the metal atom. The metal−B_{12} interactions are described by three types of bonds. First, there is one clear 4c−2e π bond between the metal and the B_3 fragment. Second, there are four totally delocalized 13c−2e bonds with ON = 2.00 lel. These four bonding elements are very interesting and they can be viewed as consisting of both σ and π interactions between the metal and the entire B_{12} moiety. Finally, there are three localized 2c−2e σ bonds between Rh and the three nearest boron atoms (ON = 1.83 lel). These three metal−boron covalent bonds are unique, quite different from the primarily ionic interactions observed previously in the C_{7v} AlB_7^-, C_{8v} AlB_8^-, or C_{8v} LiB_8^- half-sandwich complexes between the metal atom and the quasi-planar B_7 or B_8 motif.[16,19] The presented inclination to form localized bonds between metals and boron might be explained by the difference in the electronegativity values, which is almost negligible for Co and Rh atoms: 0.16 and 0.24, respectively. Significantly larger difference is seen for Al and Li atoms (0.43 and 1.06, respectively), which is responsible for the ionic interaction. We believe that electronegativity difference could be one of the useful design tools for such systems. The Co−B and Rh−B bond lengths are found to be 2.25 Å and 2.35 Å at the PBE0 level of theory in the CoB_{12}^- and RhB_{12}^- clusters, respectively. It should also be pointed out that these bonds were also revealed using the NBO analysis, which showed that the contribution of B to the metal−boron bonds are 12% and 14% for Rh and Co, respectively.

It is interesting to point out that there are only two lone pairs on the metal atom with ON = 1.92 lel. The common oxidation states of Co and Rh are II (d^7) and III (d^6).[73,74] The current bonding analyses suggest that the metal atom has a rare oxidation state of M^0 (d^9) in the MB_{12}^- complexes, even though six electrons participate in the formation of M−B bonds. Since the contribution of B to the M−B bonds is quite low, these six electrons might be considered primarily as lone pairs on the atom of metal. Furthermore, these two lone pairs provide possible sites for additional coordination by suitable ligands, which may allow the MB_{12} complexes to be synthesized in bulk. Recently, a planar B_6 cluster has been found to be sandwiched by two Ta atoms in the D_{6h} Ta_2B_6 cluster,[33] similar to the B_6 building blocks observed in a solid metal boride compound.[32] The current study demonstrates that larger planar boron clusters may also be possible as ligands or solid building blocks.

VII. CONCLUSION

We have carried out a combined experimental and theoretical study on two transition metal and B_{12} complexes, CoB_{12}^- and RhB_{12}^-. These two valence isoelectronic clusters have similar photoelectron spectral patterns, suggesting similarity of their structures. Extensive computational searches established that both CoB_{12}^- and RhB_{12}^- have C_{3v} half-sandwich global minimum structures with the B_{12} cluster coordinating to the metal atom. The B_{12} moiety in the MB_{12}^- complexes maintains a similar geometry as the bare quasiplanar B_{12} cluster, except a slightly larger out-of-planar distortion to optimize bonding with the metal atom. Chemical bonding analyses revealed strong interactions between the metal atom and the B_{12} moiety via both σ and π bonds. More significantly, the Co and Rh atoms assume a rare oxidation state of M^0 (d^9) in the MB_{12}^- complexes. The two *d*-electron lone pairs on the metal atom provide possible sites for appropriate ligands for further coordination to the metal, suggesting novel compounds with planar boron clusters as building blocks may be viable.

■ ASSOCIATED CONTENT

Supporting Information

Full citation for reference 62. Representative optimized lowest isomers of CoB_{12}^- and RhB_{12}^-, their point group symmetries, overall spectroscopic states, relative energies at the PBE0/M/Stuttgart/B/aug-cc-pVTZ and CCSD(T)/Rh/Stuttgart/B/aug-cc-pVTZ//PBE0/M/Stuttgart/B/aug-cc-pVTZ levels of theory, and Cartesian coordinates of the global minimum structures of CoB_{12}^- and RhB_{12}^- at PBE0/M/Stuttgart/B/aug-cc-pVTZ (*M* = Co, Rh). This material is available free of charge via the Internet at http://pubs.acs.org.

■ AUTHOR INFORMATION

Corresponding Authors

*E-mail: a.i.boldyrev@usu.edu.
*E-mail: lai-sheng_wang@brown.edu.

Notes

The authors declare no competing financial interest.

■ ACKNOWLEDGMENTS

This work was supported by the National Science Foundation (CHE-1263745 to L.S.W. and CHE-1057746 to A.I.B.). We thank Dr. C. Romanescu for his assistance during the experiment. Computer resources from the Division of Research Computing in the Office of Research and Graduate Studies at Utah State University are gratefully acknowledged. I.A.P. would like to give special thanks to John Hanks at the Division of Research Computing in the Office of Research and Graduate Studies at Utah State University for making special accommodations, which allowed this research to be accomplished.

■ REFERENCES

(1) Saykally, R. J. Small Carbon Clusters: Spectroscopy, Structure, and Energetics. *Chem. Rev.* **1998**, *98*, 2313−2358.

(2) Zhai, H. J.; Alexandrova, A. N.; Birch, K. A.; Boldyrev, A. I.; Wang, L. S. Hepta- and Octacoordinated Boron in Molecular Wheels of Eight- and Nine-Atom Boron Clusters: Observation and Confirmation. *Angew. Chem., Int. Ed.* **2003**, *42*, 6004−6008.
(3) Zhai, H. J.; Kiran, B.; Li, J.; Wang, L. S. Hydrocarbon Analogues of Boron Clusters - Planarity, Aromaticity and Antiaromaticity. *Nat. Mater.* **2003**, *2*, 827−833.
(4) Sergeeva, A. P.; Zubarev, D. Y.; Zhai, H. J.; Boldyrev, A. I.; Wang, L. S. A Photoelectron Spectroscopic and Theoretical Study of B_{16}^- and B_{16}^{2-}: An All-Boron Naphthalene. *J. Am. Chem. Soc.* **2008**, *130*, 7244−7246.
(5) Sergeeva, A. P.; Averkiev, B. B.; Zhai, H. J.; Boldyrev, A. I.; Wang, L. S. All-Boron Analogues of Aromatic Hydrocarbons: B_{17}^- and B_{18}^-. *J. Chem. Phys.* **2011**, *134*, 224304.
(6) Huang, W.; Sergeeva, A. P.; Zhai, H. J.; Averkiev, B. B.; Wang, L. S.; Boldyrev, A. I. A Concentric Planar Doubly π-Aromatic B_{19}^- Cluster. *Nat. Chem.* **2010**, *2*, 202−206.
(7) Piazza, Z. A.; Li, W. L.; Romanescu, C.; Sergeeva, A. P.; Wang, L. S.; Boldyrev, A. I. A Photoelectron Spectroscopy and *Ab Initio* Study of B_{21}^-: Negatively Charged Boron Clusters Continue to Be Planar at 21. *J. Chem. Phys.* **2012**, *136*, 104310.
(8) Sergeeva, A. P.; Piazza, Z. A.; Romanescu, C.; Li, W. L.; Boldyrev, A. I.; Wang, L. S. B_{22}^- and B_{23}^-: All-Boron Analogues of Anthracene and Phenanthrene. *J. Am. Chem. Soc.* **2012**, *134*, 18065−18073.
(9) Popov, I. A.; Piazza, Z. A.; Li, W. L.; Wang, L. S.; Boldyrev, A. I. A Combined Photoelectron Spectroscopy and *Ab Initio* Study of the Quasi-Planar B_{24}^- Cluster. *J. Chem. Phys.* **2013**, *139*, 144307.
(10) Kiran, B.; Bulusu, S.; Zhai, H. J.; Yoo, S.; Zeng, X. C.; Wang, L. S. Planar-to-Tubular Structural Transition in Boron Clusters: B_{20} As the Embryo of Single-Walled Boron Nanotubes. *Proc. Natl. Acad. Sci. U.S.A.* **2005**, *102*, 961.
(11) Oger, E.; Crawford, N. R. M.; Kelting, R.; Weis, P.; Kappes, M. M.; Ahlrichs, R. Boron Cluster Cations: Transition from Planar to Cylindrical Structures. *Angew. Chem., Int. Ed.* **2007**, *46*, 8503−8506.
(12) Tai, T. B.; Tam, N. M.; Nguyen, M. T. Structure of Boron Clusters Revisited, B_n with n = 14−20. *Chem. Phys. Lett.* **2012**, *530*, 71−76.
(13) Romanescu, C.; Harding, D. J.; Fielicke, A.; Wang, L. S. Probing the Structures of Neutral Boron Clusters Using Infrared/Vacuum Ultraviolet Two Color Ionization: B_{11}, B_{16}, and B_{17}. *J. Chem. Phys.* **2012**, *137*, 014317.
(14) Cheng, L. B_{14}: An All-Boron Fullerene. *J. Chem. Phys.* **2012**, *136*, 104301.
(15) Alexandrova, A. N.; Boldyrev, A. I.; Zhai, H. J.; Wang, L. S. All-Boron Aromatic Clusters as Potential New Inorganic Ligands and Building Blocks in Chemistry. *Coord. Chem. Rev.* **2006**, *250*, 2811−2866.
(16) Alexandrova, A. N.; Zhai, H. J.; Wang, L. S.; Boldyrev, A. I. Molecular Wheel B_8^{2-} as a New Inorganic Ligand. Photoelectron Spectroscopy and Ab Initio Characterization of LiB_8^-. *Inorg. Chem.* **2004**, *43*, 3552−3554.
(17) Kuznetsov, A. E.; Boldyrev, A. I. Theoretical Evidence of Aromaticity in X_3^- (X = B, Al, Ga) Species. *Struct. Chem.* **2002**, *13*, 141−148.
(18) Alexandrova, A. N.; Boldyrev, A. I.; Zhai, H. J.; Wang, L. S. Photoelectron Spectroscopy and Ab Initio Study of the Doubly Antiaromatic B_6^{2-} Dianion in the LiB_6^- Cluster. *J. Chem. Phys.* **2005**, *122*, 054313.
(19) Galeev, T. R.; Romanescu, C.; Li, W. L.; Wang, L. S.; Boldyrev, A. I. Valence Isoelectronic Substitution in the B_8^- and B_9^- Molecular Wheels by an Al Dopant Atom: Umbrella-like Structures of AlB_7^- and AlB_8^-. *J. Chem. Phys.* **2011**, *135*, 104301.
(20) Romanescu, C.; Galeev, T. R.; Li, W. L.; Boldyrev, A. I.; Wang, L. S. Transition-Metal-Centered Monocyclic Boron Wheel Clusters ($M©B_n$): A New Class of Aromatic Borometallic Compounds. *Acc. Chem. Res.* **2013**, *46*, 350−358.
(21) Romanescu, C.; Galeev, T. R.; Li, W. L.; Boldyrev, A. I.; Wang, L. S. Aromatic Metal-Centered Monocyclic Boron Rings: $Co©B_8^-$ and $Ru©B_9^-$. *Angew. Chem., Int. Ed.* **2011**, *50*, 9334−9337.
(22) Li, W. L.; Romanescu, C.; Galeev, T. R.; Piazza, Z. A.; Boldyrev, A. I.; Wang, L. S. Transition-Metal-Centered Nine-Membered Boron Rings: $M©B_9$ and $M©B_9^-$ (M = Rh, Ir). *J. Am. Chem. Soc.* **2012**, *134*, 165−168.
(23) Galeev, T. R.; Romanescu, C.; Li, W. L.; Wang, L. S.; Boldyrev, A. I. Observation of the Highest Coordination Number in Planar Species: Decacoordinated $Ta©B_{10}^-$ and $Nb©B_{10}^-$ Anions. *Angew. Chem., Int. Ed.* **2012**, *51*, 2101−2105.
(24) Romanescu, C.; Galeev, T. R.; Sergeeva, A. P.; Li, W. L.; Wang, L. S.; Boldyrev, A. I. Experimental and Computational Evidence of Octa- and Nona-Coordinated Planar Iron-Doped Boron Clusters: $Fe©B_8^-$ and $Fe©B_9^-$. *J. Organomet. Chem.* **2012**, *721−722*, 148−154.
(25) Romanescu, C.; Galeev, T. R.; Li, W. L.; Boldyrev, A. I.; Wang, L. S. Geometric and Electronic Factors in the Rational Design of Transition-Metal-Centered Boron Molecular Wheels. *J. Chem. Phys.* **2013**, *138*, 134315.
(26) Li, W. L.; Ivanov, A. S.; Federič, J.; Romanescu, C.; Černušák, I.; Boldyrev, A. I.; Wang, L. S. On the Way to the Highest Coordination Number in the Planar Metal-Centered Aromatic $Ta©B_{10}^-$ Cluster: Evolution of the Structures of TaB_n^- (n = 3−8). *J. Chem. Phys.* **2013**, *139*, 104312.
(27) Heine, T.; Merino, G. What Is the Maximum Coordination Number in a Planar Structure? *Angew. Chem., Int. Ed.* **2012**, *51*, 4275−4276.
(28) Li, L.; Xu, C.; Cheng, L. Density Functional Investigation of $X@B_nH_n$ (X = B^+, Be; n = 5−8). *Comp. Theor. Chem.* **2013**, *1021*, 144−148.
(29) Li, L.; Xu, C.; Jin, B.; Cheng, L. Benzene Analogues of (Quasi-) Planar $M@B_nH_n$ Compounds (M = V^-, Cr, Mn^+): A Theoretical Investigation. *J. Chem. Phys.* **2013**, *139*, 174310.
(30) Le Guennic, B.; Jiao, H.; Kahlal, S.; Saillard, J. Y.; Halet, J. F.; Ghosh, S.; Shang, M.; Beatty, A. M.; Rheingold, A. L.; Fehlner, T. P. Synthesis and Characterization of Hypoelectronic Rhenaboranes. Analysis of the Geometric and Electronic Structures of Species Following Neither Borane Nor Metal Cluster Electron-Counting Paradigms. *J. Am. Chem. Soc.* **2004**, *126*, 3203−3217.
(31) Ghosh, S.; Beatty, A. M.; Fehlner, T. P. Synthesis and Characterization of Bicapped Hexagonal Bipyramidal 2,3-Cl_2-1,8-$\{Cp^*Re\}_2B_6H_4[\{Cp^*Re\}]_2\{\mu$-$\eta^6$: η^6-1,2-$B_6H_4Cl_2\}$, Cp^* = η^5-C_5Me_5]: The Missing Link Connecting (p−2) Skeletal Electron Pair Hypoelectronic Rhenaboranes and 24-Valence Electron Triple-Decker Complexes. *J. Am. Chem. Soc.* **2001**, *123*, 9188−9189.
(32) Fokwa, B. P. T.; Hermus, M. All-Boron Planar B_6 Ring in the Solid-State Phase $Ti_7Rh_4Ir_2B_8$. *Angew. Chem., Int. Ed.* **2012**, *51*, 1702−1705.
(33) Li, W. L.; Xie, L.; Jian, T.; Romanescu, C. Hexagonal Bipyramidal $Ta_2B_6^{-/0}$ Clusters: B_6 Rings as Structural Motifs. *Angew. Chem., Int. Ed.*, in press.
(34) Li, W. L.; Romanescu, C.; Piazza, Z. A.; Wang, L. S. Geometrical Requirements for Transition-Metal-Centered Aromatic Boron Wheels: The Case of VB_{10}^-. *Phys. Chem. Chem. Phys.* **2012**, *14*, 13663−13669.
(35) Jia, J.; Ma, L.; Wang, J. F.; Wu, H. S. Structures and Stabilities of ScB_n (n = 1−12) Clusters: An Ab Initio Investigation. *J. Mol. Model.* **2013**, *19*, 3255−3261.
(36) Li, S. D.; Miao, C. Q.; Guo, J. C.; Ren, G. M. Transition Metal−Boron Complexes B_nM: From Bowls (n = 8−14) to Tires (n = 14). *J. Comput. Chem.* **2006**, *27*, 1858−1865.
(37) Wang, L. S.; Cheng, H. S.; Fan, J. W. Photoelectron Spectroscopy of Size-Selected Transition Metal Clusters: Fe_n^-, n = 3−24. *J. Chem. Phys.* **1995**, *102*, 9480−9493.
(38) Akola, J.; Manninen, M.; Hakkinen, H.; Landman, U.; Li, X.; Wang, L. S. Photoelectron Spectra of Aluminum Cluster Anions: Temperature Effects and Ab Initio Simulations. *Phys. Rev. B* **1999**, *60*, R11297−R11300.
(39) Huang, W.; Wang, L. S. Probing the 2D to 3D Structural Transition in Gold Cluster Anions Using Argon Tagging. *Phys. Rev. Lett.* **2009**, *102*, 153401.

(40) Adamo, C.; Barone, V. Toward Reliable Density Functional Methods Without Adjustable Parameters: The PBE0Model. *J. Chem. Phys.* **1999**, *110*, 6158−6170.
(41) Perdew, J. P.; Burke, K.; Ernzerhof, M. Generalized Gradient Approximation Made Simple. *Phys. Rev. Lett.* **1996**, *77*, 3865−3868.
(42) Hay, P. J.; Wadt, W. R. Ab Initio Effective Core Potentials for Molecular Calculations - Potentials for the Transition-Metal Atoms Sc to Hg. *J. Chem. Phys.* **1985**, *82*, 270−283.
(43) Kendall, R. A.; Dunning, T. H.; Harrison, R. J. Electron Affinities of the First-Row Atoms Revisited. Systematic Basis Sets and Wave Functions. *J. Chem. Phys.* **1992**, *96*, 6796−6806.
(44) Dunning, T. H. Gaussian-Basis Sets for Use in Correlated Molecular Calculations 0.1. The Atoms Boron through Neon and Hydrogen. *J. Chem. Phys.* **1989**, *90*, 1007−1023.
(45) Bergner, A.; Dolg, M.; Kuchle, W.; Stoll, H.; Preuss, H. Ab-Initio Energy-Adjusted Pseudopotentials for Elements of Groups 13−17. *Mol. Phys.* **1993**, *80*, 1431−1441.
(46) Kaupp, M.; Schleyer, P. v. R.; Stoll, H.; Preuss, H. Pseudopotential Approaches to Ca, Sr, and Ba Hydrides. Why Are Some Alkaline Earth MX_2 Compounds Bent? *J. Chem. Phys.* **1991**, *94*, 1360−1366.
(47) Dolg, M.; Stoll, H.; Preuss, H.; Pitzer, R. M. Relativistic and Correlation-Effects for Element 105 (Hahnium, Ha) - A Comparative-Study of M and Mo (M = Nb, Ta, Ha) Using Energy-Adjusted Abinitio Pseudopotentials. *J. Phys. Chem.* **1993**, *97*, 5852−5859.
(48) Becke, A. D. Density-Functional Exchange-Energy Approximation with Correct Asymptotic-Behavior. *Phys. Rev. A* **1988**, *38*, 3098−3100.
(49) Perdew, J. P. Density-Functional Approximation for the Correlation-Energy of the Inhomogeneous Electron-Gas. *Phys. Rev. B* **1986**, *33*, 8822−8824.
(50) Zhai, H. J.; Li, S.; Dixon, D. A.; Wang, L. S. Probing the Electronic and Structural Properties of Chromium Oxide Clusters $(CrO_3)_n^-$ and $(CrO_3)_n$ (n = 1−5): Photoelectron Spectroscopy and Density Functional Calculations. *J. Am. Chem. Soc.* **2008**, *130*, 5167−5177.
(51) Li, S.; Zhai, H. J.; Wang, L. S.; Dixon, D. A. Structural and Electronic Properties of Reduced Transition Metal Oxide Clusters, M_4O_{10} and $M_4O_{10}^-$ (M = Cr, W), from Photoelectron Spectroscopy and Quantum Chemical Calculations. *J. Phys. Chem. A* **2012**, *116*, 5256−5271.
(52) Zubarev, D. Y.; Boldyrev, A. I. Developing Paradigms of Chemical Bonding: Adaptive Natural Density Partitioning. *Phys. Chem. Chem. Phys.* **2008**, *10*, 5207−5217.
(53) Popov, I. A.; Boldyrev, A. I. Deciphering Chemical Bonding in a BC_3 Honeycomb Epitaxial Sheet. *J. Phys. Chem. C* **2012**, *116*, 3147−3152.
(54) Popov, I. A.; Bozhenko, K. V.; Boldyrev, A. I. Is Graphene Aromatic? *Nano Res.* **2012**, *5*, 117−123.
(55) Popov, I. A.; Li, Y.; Chen, Z.; Boldyrev, A. I. "Benzation" of Graphene upon Addition of Monovalent Chemical Species. *Phys. Chem. Chem. Phys.* **2013**, *15*, 6842−6848.
(56) Foster, J. P.; Weinhold, F. Natural Hybrid Orbitals. *J. Am. Chem. Soc.* **1980**, *102*, 7211−7218.
(57) Reed, A. E.; Curtiss, L. A.; Weinhold, F. Intermolecular Interactions from a Natural Bond Orbital, Donor−Acceptor Viewpoint. *Chem. Rev.* **1988**, *88*, 899−926.
(58) Van Lenthe, E.; Baerends, E. J. Optimized Slater-Type Basis Sets for the Elements 1−118. *J. Comput. Chem.* **2003**, *24*, 1142−1156.
(59) te Velde, G.; Bickelhaupt, F. M.; Baerends, E. J.; Guerra, C. F.; Van Gisbergen, S. J. A.; Snijders, J. G.; Ziegler, T. Chemistry with ADF. *J. Comput. Chem.* **2001**, *22*, 931−967.
(60) Guerra, C. F.; Snijders, J. G.; te Velde, G.; Baerends, E. J. Towards an Order-N DFT Method. *Theor. Chem. Acc.* **1998**, *99*, 391−403.
(61) *ADF 2010*; SCM, Theoretical Chemistry, Vrije Universiteit: Amsterdam, The Netherlands, 2010 (http://www.scm.com).
(62) Frisch, M. J. et al. *Gaussian 09*, revision A.1; Gaussian, Inc.: Wallingford, CT, 2009.
(63) Schaftenaar, G. *MOLDEN 3.4*; CAOS/CAMM Center: Nijmegen, The Netherlands, 1998.
(64) See http://www.chemcraftprog.com for the description of the Chemcraft program.
(65) Varetto, U. *Molekel 5.4.0.8*; Swiss National Supercomputing Centre: Manno, Switzerland, 2011.
(66) Jayatilaka, D.; Lee, T. J. Open-Shell Coupled-Cluster Theory. *J. Chem. Phys.* **1993**, *98*, 9734−9747.
(67) Lee, T. J.; Rice, J. E.; Scuseria, G. E.; Schaefer, H. F. Theoretical Investigations of Molecules Composed Only of Fluorine, Oxygen and Nitrogen: Determination of the Equilibrium Structures of FOOF, $(NO)_2$ and FNNF and the Transition-State Structure for FNNF *cis*−*trans* Isomerization. *Theor. Chim. Acta.* **1989**, *75*, 81−98.
(68) Lee, T. J.; Taylor, P. R. A Diagnostic for Determining the Quality of Single-Reference Electron Correlation Methods. *Int. J. Quantum Chem.* **1989**, 199−207.
(69) Fowler, J. E.; Ugalde, J. M. The Curiously Stable B_{13}^+ Cluster and Its Neutral and Anionic Counterparts: The Advantages of Planarity. *J. Phys. Chem. A* **2000**, *104*, 397−403.
(70) Gu, F. L.; Yang, X. M.; Tang, A. C.; Jiao, H. J.; Schleyer, P. V. Structure and Stability of B_{13}^+ Clusters. *J. Comput. Chem.* **1998**, *19*, 203−214.
(71) Martinez-Guajardo, G.; Sergeeva, A. P.; Boldyrev, A. I.; Heine, T.; Ugalde, J. M.; Merino, G. Unraveling the Phenomenon of Internal Rotation in B_{13}^+ through Chemical Bonding Analysis. *Chem. Commun.* **2011**, *47*, 6242−6244.
(72) Jimenez-Halla, J. O. C.; Islas, R.; Heine, T.; Merino, G. B_{19}^-: An Aromatic Wankel Motor. *Angew. Chem., Int. Ed.* **2010**, *49*, 5668−5671.
(73) Leavason, W.; McAuliffe, C. A. High Oxidation State Chemistry of Iron, Cobalt, and Nickel. *Coord. Chem. Rev.* **1974**, *12*, 151−184.
(74) Cotton, F. A.; Wilkinson, G. *Advanced Inorganic Chemistry*, 5th ed.; Wiley: New York, 1988.